INTERNATIONAL JOURNAL OF
NUMERICAL ANALYSIS AND MODELING
Volume 19, Number 1, Pages 85–100

A SCALAR AUXILIARY VARIABLE (SAV) AND OPERATOR SPLITTING COMPACT FINITE DIFFERENCE METHOD FOR PERITECTIC PHASE FIELD MODEL

JIAJIE FEI, SHUSEN XIE, AND CHUNGUANG CHEN*

Abstract. Peritectic crystallization is a process in which the solid phase precipitated in the form of solid solution reacts with the liquid phase to form another solid phase. The process can be described by a phase field model where two continuous phase variables, ϕ and ψ, are introduced to distinguish the three different phases. We discretize the time variable with a scalar auxiliary variable (SAV) method that can ensure the unconditional energy stability. Moreover, the SAV method only requires solving a linear system at each time step and therefore reduces the computational complexity. The space variables in a two-dimensional region are discretized by an operator splitting method equipped with a high order compact finite difference formulation. This approach is effective and convenient since only a series one-dimensional problems need to be solved at each step. We prove the unconditional energy stability theoretically and test the order of convergence and energy stability through numerical experiments. Simulations of peritectic solidification demonstrate the patterns formed during the process.

Key words. Peritectic crystallization, phase field model, scalar auxiliary variable (SAV) method, operator splitting, compact finite difference method.

1. Introduction

Peritectic crystallization occurs when the solution of alloy is cooled down to critical temperature and one solid phase, denoted by α, precipitated in the form of solid solution reacts with the liquid phase to form another solid phase, denoted by β. This process is similar to eutectic crystallization where the two different solid phases precipitated simultaneously from the solution. The mathematical modeling of both processes has gradually matured with the application of phase field model. In a typical phase field model, a variable, usually denoted by ϕ, takes two different values in solid and liquid, e.g. $+1$ and -1, changes smoothly between the two values in the region around the interface and diffuses with a limited width. Another variable, ψ, is used to distinguish the α-solid and β-solid in the same way. The discrete position of the interface can be defined as the set of all points where the phase field takes a specific value, e.g. 0. In other words, the phase field model does not track the location of the interface explicitly, unlike the sharp-interface approach such as level-set method, hence is effective in simulations of complicated patterns formed in alloy solidification.

Concerning the peritectic process, Trivedi [26] proposed a one-dimensional model to explain the formation of peritectic banded structure in pure diffusion controlled growth. This model is improved by P. Mazumder, R. Trivedi and A. Karma [20] under the assumption of a planar solidification front and incorporation with a fully two-dimensional convection flow field. A. Wheeler et al [29] proposed a phase field model for eutectic solidification which is then developed for both eutectic and peritectic phase transitions [21]. Based on [29], T. S. Lo, A. Karma and M. Plapp

Received by the editors January 28, 2021 and, in revised form, May 7, 2021.
2000 *Mathematics Subject Classification.* 65M06, 65M12, 65P99, 35Q99.
*Corresponding author. Email: cgchen@ouc.edu.cn.

[19] developed a phase field model of the formation of microstructure mode during directional solidification of amorphous unstable peritectic alloys. This model will be discussed and solved numerically in the following sections.

As the evolution of phase field model is driven by energy dissipation, it is crucial to imitate this physical law in numerical approximation. Numerical schemes that satisfy discrete energy dissipation law are energy stable. X. Yang and D. Han [32] developed a series of linear, unconditionally energy stable numerical schemes for solving the phase field crystal model. The temporal discretizations are based on the first order Euler method, the second order backward differentiation formulas (BDF2) and the second order Crank-Nicolson method, respectively. K. Cheng, W. Feng and C. Wang [4] proposed an energy stable numerical scheme for the Cahn-Hilliard equation by the long stencil fourth order finite difference approximation. In the temporal approximation, a second order BDF stencil is applied with a second order extrapolation formula applied to the concave diffusion term, as well as a second order artificial Douglas-Dupont regularization term, for the sake of energy stability. K. Cheng, C. Wang and S. M. Wise [5] proposed an energy stable numerical scheme for the strongly anisotropic Cahn-Hilliard model that is discretized in space by the Fourier pseudospectral method. C. Elliott and A. Stuart [11] construct an energy stable scheme with the convex splitting method that was applied to solve Cahn-Hilliard equation by D. Eyre [12]. W. Chen et al [3] combined the convex splitting method with a variable step BDF-2 approach and mixed finite element method to approximate the Cahn-Hilliard equation and obtained second order rate of convergence. Although the convex splitting method is unconditionally energy stable, a nonlinear system has to be solved at every time level. J. Zhu et al [37] proposed an efficient numerical method for the phase field model that maintains the energy stability by adding an artificial stabilization term. However, this approach is difficult to extend to high-order schemes.

F. Guilln-Gonzlez and G. Tierra [15, 2] proposed the invariant energy quadratization (IEQ) method to solve the interface diffusion problem. The IEQ method can be effectively extended to the higher-order schemes and only require solving linear systems with variable coefficients at each time step [31]. The IEQ method is then developed by J. Shen [23, 24] to scalar auxiliary variable (SAV) method and is widely used in numerical approximations for phase field and related problems [1, 6, 13, 34, 35, 28, 36]. In addition to maintaining unconditional energy stability, only linear systems with *constant* coefficients need to be solved at each step. And, unlike IEQ method, the SAV approach reduces the system to *de-coupled* Poisson type equations for multi-component models. In this paper, we apply the SAV method for time discretization in the numerical approximations of the peritectic phase transition.

To account for the two-dimensional space variable, we implement an operator splitting approach equipped with a high order compact finite difference scheme [14, 30]. The 2D Poisson problem is separated into two 1D equations that are solved by fourth-order compact finite difference schemes. The operator splitting method has been widely used to approximate high dimensional problems. C. Zhang et al [33] proved the nonlinear stability and convergence of a second-order operator splitting scheme applied to the "good" Boussinesq equation. Y. Cheng et al [7] proposed a fast explicit operator splitting method for the epitaxial growth model with slope selection. This approach is modified by X. Li, Z. Qiao and H. Zhang [16] with a compact center-difference scheme. C. Liu, C. Wang and Y. Wang [17] suggested a

positivity-preserving, energy stable operator splitting scheme for reaction-diffusion equations with detailed balance.

The advantage of compact finite difference method lies in efficient approximations of derivatives with short stencils. W. E and J. Liu [10] suggested an essentially compact schemes for unsteady viscous incompressible flows. J. Liu, C. Wang and H. Johnston [18] proposed a fourth order finite difference method for solving the vorticity flow function of two-dimensional unsteady viscous incompressible Boussinesq equation. C. Wang, J. Liu and H. Johnston [27] established the convergence of a fourth order finite difference method for the 2-D unsteady, viscous incompressible Boussinesq equations by using compact fourth order scheme and long-stencil fourth order operators.

The rest of this paper is organized as follows. The phase field model is introduced in Section 2. In Section 3, we discuss the numerical scheme in which we discretize the time variable by SAV method and the space variable by operator splitting compact finite difference method. Unconditional energy stability of the scheme is also proved. In Section 4, we test the rate of convergence and stability of the scheme through numerical experiments and simulate various patterns formed in the processes of peritectic crystallization. Section 5 summarizes the results of this paper.

2. The phase field model of peritectic crystallization

The phase field model for peritectic crystallization with diffusion effect on a two-dimensional domain Ω is given by [19]

$$\begin{aligned} \frac{\partial \phi}{\partial t} &= \Delta \phi - f_\phi, \\ \frac{\partial \psi}{\partial t} &= \Delta \psi - f_\psi, \\ \frac{\partial c}{\partial t} &= \frac{\alpha}{\lambda} \nabla \cdot [D(\phi) \nabla f_c], \end{aligned} \tag{1}$$

where $\phi = \phi(x, y, t)$, $(x, y) \in \Omega$, is the partition variable of solid ($\phi = 1$) and liquid ($\phi = -1$) in the crystallization process and the level curve $\phi = 0$ represents the solid-liquid interface. $\psi = \psi(x, y, t)$ is the partition variable of the two different solids α ($\psi = 1$) and β ($\psi = -1$) with the interface defined by $\psi = 0$ when ϕ is positive. The scaled composition is taken as

$$c(x, y, t) = \frac{C(x, y, t) - C_{p\beta}}{C_p - C_{p\alpha}}, \tag{2}$$

where $C = C(x, y, t)$ is the composition of the impurity and $C_p, C_{p\alpha}, C_{p\beta}$ are constants given in Table 1. For physical discussions of these constants, we refer to [19] and the references therein. α, λ are positive constants and $D(\phi) = (1 - \phi)/2$ is the diffusion coefficient that implies diffusion effect of the solute impurities becomes weaker as solidification goes on. f_ϕ, f_ψ, f_c are the partial derivatives of f to the subscript where $f = f(\phi, \psi, c)$ is the bulk free energy density of the alloy that takes the from [19]

$$\begin{aligned} f(\phi, \psi, c) = \frac{\lambda}{2} \{ c + A_1 h(\phi) + \frac{1}{2} A_2 [1 + h(\phi)] h(\psi) \}^2 \\ - \lambda \{ B_1 h(\phi) + \frac{1}{2} B_2 [1 + h(\phi)] h(\psi) \} + g(\phi) \\ + \frac{1}{2} [1 + h(\phi)] g(\psi) + \frac{1}{2} [1 - h(\phi)] \psi^2, \end{aligned}$$

where A_1, A_2 are constants and B_1, B_2 are functions of temperature.

$$g(\phi) = 1/4 - \phi^2/2 + \phi^4/4$$

is the double-well function with minima at $\phi = \pm 1$ and

$$h(\phi) = 3(\phi - \phi^3/3)/2$$

satisfies $h(\pm 1) = \pm 1, h'(\pm 1) = 0$. The functions $g(\psi)$ and $h(\psi)$ are defined in the same way. In order to relate the parameters in our model to a physical system, we take

$$\begin{aligned} B_1 &= B_{11} + B_{12}T, \\ B_2 &= B_{21} + B_{22}T, \end{aligned}$$

where T is temperature, and $B_{11}, B_{12}, B_{21}, B_{22}$ are constants.

The phase field model (1) is driven by the dissipation of Helmholtz free energy

$$F = \int_\Omega \frac{1}{2}W_\phi^2|\nabla\phi|^2 + \frac{1}{2}W_\psi^2|\nabla\psi|^2 + f(\phi,\psi,c)dx, \tag{3}$$

where W_ϕ, W_ψ are constants, determining the width of the diffusive interfaces.

3. Numerical methods for the peritectic phase field model

3.1. Time discretization by scalar auxiliary variable (SAV) method. In this section, we employ a second-order, unconditionally energy stable approach of SAV [23] for (1). For simplicity, we consider the problem on rectangular domain Ω with periodic boundary conditions. We define a scalar auxiliary variable r as follows:

$$r = \sqrt{E_1(t) + C_0},$$

where C_0 is constant that ensures the radicand positive and $E_1(t) = \int_\Omega f(\phi,\psi,c)dx$.

The phase field system (1) can be rewritten as

$$\begin{aligned} \frac{\partial\phi}{\partial t} &= \Delta\phi - \frac{r}{\sqrt{E_1 + C_0}}f_\phi, \\ \frac{\partial\psi}{\partial t} &= \Delta\psi - \frac{r}{\sqrt{E_1 + C_0}}f_\psi, \\ \frac{\partial c}{\partial t} &= \frac{\alpha}{\lambda}\nabla\cdot\left[D(\phi)\nabla\left(\frac{r}{\sqrt{E_1 + C_0}}f_c\right)\right], \\ \frac{dr}{dt} &= \frac{1}{2\sqrt{E_1 + C_0}}\int_\Omega f_\phi\phi_t + f_\psi\psi_t + f_c c_t dx, \end{aligned} \tag{4}$$

where ϕ_t, ψ_t, c_t represent the derivatives of ϕ, ψ, c with respect to t.

Let Δt be the time step and $\phi^n = \phi(n\Delta t)$, then we can discretize the above system in time by the second order backward difference formula (BDF-2) to obtain

a semi-discrete scheme

$$
\begin{aligned}
&\frac{3\phi^{n+1}-4\phi^{n}+\phi^{n-1}}{2\Delta t}=\Delta\phi^{n+1}-\frac{r^{n+1}}{\sqrt{E_1^{n+1/2}+C_0}}f_\phi^{n+1/2},\\
&\frac{3\psi^{n+1}-4\psi^{n}+\psi^{n-1}}{2\Delta t}=\Delta\psi^{n+1}-\frac{r^{n+1}}{\sqrt{E_1^{n+1/2}+C_0}}f_\psi^{n+1/2},\\
&\frac{3c^{n+1}-4c^{n}+c^{n-1}}{2\Delta t}=\frac{\alpha}{\lambda}\nabla\cdot\left[D(\phi^{n+1/2})\nabla\left(\frac{r^{n+1}}{\sqrt{E_1^{n+1/2}+C_0}}f_c^{n+1/2}\right)\right],\\
&\frac{3r^{n+1}-4r^{n}+r^{n-1}}{2\Delta t}=\frac{1}{2\sqrt{E_1^{n+1/2}+C_0}}\int_\Omega f_\phi^{n+1/2}\frac{3\phi^{n+1}-4\phi^{n}+\phi^{n-1}}{2\Delta t}\\
&+f_\psi^{n+1/2}\frac{3\psi^{n+1}-4\psi^{n}+\psi^{n-1}}{2\Delta t}+f_c^{n+1/2}\frac{3c^{n+1}-4c^{n}+c^{n-1}}{2\Delta t}dx,
\end{aligned}
\tag{5}
$$

here $E_1^{n+1/2}=\int_\Omega f(\phi^{n+1/2},\psi^{n+1/2},c^{n+1/2})dx$, $f_\phi^{n+1/2}=f_\phi(\phi^{n+1/2},\psi^{n+1/2},c^{n+1/2})$, $f_\psi^{n+1/2}=f_\psi(\phi^{n+1/2},\psi^{n+1/2},c^{n+1/2})$ and $f_c^{n+1/2}=f_c(\phi^{n+1/2},\psi^{n+1/2},c^{n+1/2})$ are second-order approximations for $E_1^{n+1},f_\phi^{n+1},f_\psi^{n+1}$ and f_c^{n+1}, respectively. $\phi^{n+1/2}$, $\psi^{n+1/2}$, $c^{n+1/2}$ are implicit second-order approximations for $\phi^{n+1},\psi^{n+1},c^{n+1}$, respectively, obtained by solving the following system:

$$
\begin{aligned}
&\frac{\phi^{n+1/2}-\phi^{n}}{\Delta t}=\Delta\phi^{n+1/2}-f_\phi(\phi^{n},\psi^{n},c^{n}),\\
&\frac{\psi^{n+1/2}-\psi^{n}}{\Delta t}=\Delta\psi^{n+1/2}-f_\psi(\phi^{n},\psi^{n},c^{n}),\\
&\frac{c^{n+1/2}-c^{n}}{\Delta t}=\frac{\alpha}{\lambda}\nabla\cdot\left[D(\phi^{n+1/2})\nabla f_c(\phi^{n},\psi^{n},c^{n})\right].
\end{aligned}
\tag{6}
$$

Denote

$$
b_\lambda^n=\frac{f_\lambda^{n+1/2}}{\sqrt{E_1^{n+1/2}+C_0}},\quad\text{with}\quad\lambda=\phi,\psi,c.
$$

The first equation in (5) can be written as

$$
\left(I-\frac{2}{3}\Delta t\Delta\right)\phi^{n+1}=-\frac{2}{3}\Delta t b_\phi^n r^{n+1}+\frac{4}{3}\phi^{n}-\frac{1}{3}\phi^{n-1}.
\tag{7}
$$

Let $(f(x),g(x))=\int_\Omega f(x)g(x)dx$ be the inner product on Ω and the last equation in (5) can be written as

$$
r^{n+1}=\frac{1}{2}\left[(b_\phi^n,\phi^{n+1})+(b_\psi^n,\psi^{n+1})+(b_c^n,c^{n+1})\right]+p^n,
\tag{8}
$$

where

$$
\begin{aligned}
p^n=&\frac{1}{6}\left[(b_\phi^n,-4\phi^{n}+\phi^{n-1})+(b_\psi^n,-4\psi^{n}+\psi^{n-1})\right.\\
&\left.+(b_c^n,-4c^{n}+c^{n-1})\right]+\frac{4}{3}r^{n}-\frac{1}{3}r^{n-1}.
\end{aligned}
$$

Plugging (8) into (7) to obtain that

$$\begin{aligned}&\left(I-\frac{2}{3}\Delta t\Delta\right)\phi^{n+1}+\frac{1}{3}\Delta t\left[(b_\phi^n,\phi^{n+1})+(b_\psi^n,\psi^{n+1})+(b_c^n,c^{n+1})\right]b_\phi^n\\&=-\frac{2}{3}\Delta t p^n b_\phi^n+\frac{4}{3}\phi^n-\frac{1}{3}\phi^{n-1}.\end{aligned}\tag{9}$$

Let

$$A=I-\frac{2}{3}\Delta t\Delta,$$
$$g_\phi^n=-\frac{2}{3}\Delta t p^n b_\phi^n+\frac{4}{3}\phi^n-\frac{1}{3}\phi^{n-1},$$
$$\theta^n=(b_\phi^n,\phi^{n+1})+(b_\psi^n,\psi^{n+1})+(b_c^n,c^{n+1}),$$

and

$$v_1^n=A^{-1}b_\phi^n,\quad w_1^n=A^{-1}g_\phi^n.$$

Then (9) can be written as the equivalent form

$$\phi^{n+1}+\frac{1}{3}\Delta t v_1^n\theta^n=w_1^n.\tag{10}$$

Taking inner product of both sides with b_ϕ^n to obtain that

$$(b_\phi^n,\phi^{n+1})+\frac{1}{3}\Delta t\theta^n(b_\phi^n,v_1^n)=(b_\phi^n,w_1^n).\tag{11}$$

Similarly, we can get the equations for ψ^{n+1}:

$$\psi^{n+1}+\frac{1}{3}\Delta t\theta^n v_2^n=w_2^n,\tag{12}$$

$$(b_\psi^n,\psi^{n+1})+\frac{1}{3}\Delta t\theta^n(b_\psi^n,v_2^n)=(b_\psi^n,w_2^n),\tag{13}$$

where $v_2^n=A^{-1}b_\psi^n$, $w_2^n=A^{-1}g_\psi^n$. Moreover, the third equation in (5) can be written as

$$c^{n+1}=\frac{2\alpha}{3\lambda}\Delta t\nabla\cdot(D^{n+1/2}\nabla b_c^n)r^{n+1}+\frac{4}{3}c^n-\frac{1}{3}c^{n-1},$$

where $D^{n+1/2}=D(\phi^{n+1/2})$.

Plugging (8) into the above equation gives

$$c^{n+1}-\frac{\alpha\theta^n}{3\lambda}\Delta t\nabla\cdot(D^{n+1/2}\nabla b_c^n)=\frac{2\alpha}{3\lambda}\Delta t\nabla\cdot(D^{n+1/2}\nabla b_c^n)p^n+\frac{4}{3}c^n-\frac{1}{3}c^{n-1}.\tag{14}$$

Let $g_c^n=\frac{2\alpha}{3\lambda}\Delta t\nabla\cdot(D^{n+1/2}\nabla b_c^n)p^n+\frac{4}{3}c^n-\frac{1}{3}c^{n-1}$ and take inner product of both sides with b_c^n to obtain that

$$(b_c^n,c^{n+1})+\frac{\alpha\theta^n}{3\lambda}\Delta t(D^{n+1/2}\nabla b_c^n,\nabla b_c^n)=(b_c^n,g_c^n).\tag{15}$$

Denote

$$\gamma^n=\frac{1}{3}\Delta t(b_\phi^n,v_1^n)+\frac{1}{3}\Delta t(b_\psi^n,v_2^n)+\frac{\alpha}{3\lambda}\Delta t(D^{n+1/2}\nabla b_c^n,\nabla b_c^n),\tag{16}$$

and sum up the equations (11), (13) and (15) to get

$$\theta^n(1+\gamma^n)=(b_\phi^n,w_1^n)+(b_\psi^n,w_2^n)+(b_c^n,g_c^n).\tag{17}$$

The solutions for the semi-discrete system (5) can be found with the following steps:

(i) Compute γ^n with (16), which requires to solve the decoupled second-order equations $Av_1^n=b_\phi^n$ and $Av_2^n=b_\psi^n$.

(ii) Compute θ^n with (17), which requires to solve the decoupled second-order equations $Aw_1^n = g_\phi^n$ and $Aw_2^n = g_\psi^n$.

(iii) Use $\theta^n, v_1^n, v_2^n, w_1^n$ and w_2^n found in (i) and (ii) to compute the solution $\phi^{n+1}, \psi^{n+1}, c^{n+1}$ by (10), (12) and (14).

Hence, the key problem we need to solve is the elliptic equation $Au = g$ which will be approximated in next section through an operator splitting scheme combined with a high-precision compact finite difference method.

Next, we discuss the energy stability of the scheme (5).

Theorem 2.1. The scheme (5) is unconditionally energy stable which satisfies the following discrete energy dissipation law,

$$\frac{1}{\Delta t}(E^{n+1} - E^n) \le 0,$$

where

$$\begin{aligned} E^{n+1} =& \frac{1}{2}\left(|r^{n+1}|^2 + |2r^{n+1} - r^n|^2\right) + \frac{1}{4}\left(\|\nabla\phi^{n+1}\|^2 + \|2\nabla\phi^{n+1} - \nabla\phi^n\|^2\right) \\ &+ \frac{1}{4}\left(\|\nabla\psi^{n+1}\|^2 + \|2\nabla\psi^{n+1} - \nabla\psi^n\|^2\right). \end{aligned} \tag{18}$$

Proof. Let

$$\xi^{n+1} = \Delta\phi^{n+1} - \frac{r^{n+1}}{\sqrt{E_1^{n+1/2} + C_0}} f_\phi^{n+1/2}, \tag{19}$$

$$\eta^{n+1} = \Delta\psi^{n+1} - \frac{r^{n+1}}{\sqrt{E_1^{n+1/2} + C_0}} f_\psi^{n+1/2}. \tag{20}$$

Then we have, by the first two equations in (5), that

$$\begin{aligned} \frac{3\phi^{n+1} - 4\phi^n + \phi^{n-1}}{2\Delta t} &= \xi^{n+1}, \\ \frac{3\psi^{n+1} - 4\psi^n + \psi^{n-1}}{2\Delta t} &= \eta^{n+1}. \end{aligned}$$

Take inner product of (19) and (20) with ξ^{n+1} and η^{n+1}, respectively, to show that

$$\begin{aligned} \left(\xi^{n+1}, \frac{r^{n+1}}{\sqrt{E_1^{n+1/2} + C_0}} f_\phi^{n+1/2}\right) =& -\left(\xi^{n+1}, \xi^{n+1}\right) \\ &+ \left(\Delta\phi^{n+1}, \frac{3\phi^{n+1} - 4\phi^n + \phi^{n-1}}{2\Delta t}\right), \\ \left(\eta^{n+1}, \frac{r^{n+1}}{\sqrt{E_1^{n+1/2} + C_0}} f_\psi^{n+1/2}\right) =& -\left(\eta^{n+1}, \eta^{n+1}\right) \\ &+ \left(\Delta\psi^{n+1}, \frac{3\psi^{n+1} - 4\psi^n + \psi^{n-1}}{2\Delta t}\right). \end{aligned}$$

Similarly, taking inner product of both sides of the third equation in (5) with $\frac{r^{n+1}}{\sqrt{E_1^{n+1/2}+C_0}} f_c^{n+1/2}$ gives

$$\begin{aligned}
&\left(\frac{3c^{n+1}-4c^n+c^{n-1}}{2\Delta t}, \frac{r^{n+1}}{\sqrt{E_1^{n+1/2}+C_0}} f_c^{n+1/2}\right) \\
&= \frac{\alpha}{\lambda}\left(\nabla\cdot\left[D(\phi^{n+1/2})\nabla\left(\frac{r^{n+1}}{\sqrt{E_1^{n+1/2}+C_0}} f_c^{n+1/2}\right)\right], \frac{r^{n+1}}{\sqrt{E_1^{n+1/2}+C_0}} f_c^{n+1/2}\right) \\
&= -\frac{\alpha}{\lambda}\left(D(\phi^{n+1/2})\nabla\left(\frac{r^{n+1}}{\sqrt{E_1^{n+1/2}+C_0}} f_c^{n+1/2}\right), \nabla\left(\frac{r^{n+1}}{\sqrt{E_1^{n+1/2}+C_0}} f_c^{n+1/2}\right)\right).
\end{aligned}$$

Then multiply the last equation in (5) by $2r^{n+1}$ and substitute the above equalities to show that

$$\begin{aligned}
2r^{n+1}\frac{3r^{n+1}-4r^n+r^{n-1}}{2\Delta t} &= -\|\xi^{n+1}\|^2 + \left(\Delta\phi^{n+1}, \frac{3\phi^{n+1}-4\phi^n+\phi^{n-1}}{2\Delta t}\right) \\
&\quad -\|\eta^{n+1}\|^2 + \left(\Delta\psi^{n+1}, \frac{3\psi^{n+1}-4\psi^n+\psi^{n-1}}{2\Delta t}\right) \\
-\frac{\alpha}{\lambda}\left(D(\phi^{n+1/2})\nabla\left(\frac{r^{n+1}}{\sqrt{E_1^{n+1/2}+C_0}} f_c^{n+1/2}\right), \nabla\left(\frac{r^{n+1}}{\sqrt{E_1^{n+1/2}+C_0}} f_c^{n+1/2}\right)\right) &\\
\le \left(\Delta\phi^{n+1}, \frac{3\phi^{n+1}-4\phi^n+\phi^{n-1}}{2\Delta t}\right) + \left(\Delta\psi^{n+1}, \frac{3\psi^{n+1}-4\psi^n+\psi^{n-1}}{2\Delta t}\right),&
\end{aligned}$$

where $\alpha, \lambda, D(\phi^{n+1/2}) \ge 0$. Therefore,

$$\begin{aligned}
2r^{n+1}\frac{3r^{n+1}-4r^n+r^{n-1}}{2\Delta t} &+ \left(\nabla\phi^{n+1}, \nabla\frac{3\phi^{n+1}-4\phi^n+\phi^{n-1}}{2\Delta t}\right) \\
&+ \left(\nabla\psi^{n+1}, \nabla\frac{3\psi^{n+1}-4\psi^n+\psi^{n-1}}{2\Delta t}\right) \le 0.
\end{aligned}$$

Notice that

$$\begin{aligned}
2(a^{n+1}, 3a^{n+1}-4a^n+a^{n-1}) &= |a^{n+1}|^2 + |2a^{n+1}-a^n|^2 \\
&+|a^{n+1}-2a^n+a^{n-1}|^2 - |a^n|^2 - |2a^n-a^{n-1}|^2,
\end{aligned}$$

by dropping the positive middle term, we have

$$\begin{aligned}
&\frac{1}{2\Delta t}\left(|r^{n+1}|^2 + |2r^{n+1}-r^n|^2 - |r^n|^2 - |2r^n-r^{n-1}|^2\right) \\
&+ \frac{1}{4\Delta t}\left(\|\nabla\phi^{n+1}\|^2 + \|2\nabla\phi^{n+1}-\nabla\phi^n\|^2 - \|\nabla\phi^n\|^2 - \|2\nabla\phi^n-\nabla\phi^{n-1}\|^2\right) \\
&+ \frac{1}{4\Delta t}\left(\|\nabla\psi^{n+1}\|^2 + \|2\nabla\psi^{n+1}-\nabla\psi^n\|^2 - \|\nabla\psi^n\|^2 - \|2\nabla\psi^n-\nabla\psi^{n-1}\|^2\right) \le 0,
\end{aligned}$$

which is the desired result. □

3.2. Spatial discretization by operator splitting compact finite difference method. In Section 2.2, the phase field model (4) is disretized in time with an

SAV method. In order to compute the numerical solution, we still need to solve the Poisson type problem:

$$Au = g, \tag{21}$$

on a 2D domain $\Omega = (a_1, b_1) \times (a_2, b_2)$, where $A = I - \frac{2}{3}\Delta t\Delta$, $u = u(x, y)$ is the unknown function and $g = g(x, y)$ is given.

The domain $\{(x, y)|(x, y) \in \overline{\Omega}\}$ is discretized into grids described by the set (x_i, y_j) of nodes, in which $x_i = a_1 + ih_x$, $y_j = b_1 + jh_y$, $i = 0, 1, ..., N_x$, $j = 0, 1, ..., N_y$, where h_x, h_y are the discretization parameters. Let $v_{i,j} = v(x_i, y_j)$, $\overline{\Omega}_h = \{(x_i, y_j)|i = 0, 1, ..., N_x, j = 0, 1, ..., N_y\}$. We will use the following notations for difference operators:

$$\begin{aligned}
&\delta_{\tilde{x}} v_{i,j} = \frac{v_{i+1,j} - v_{i-1,j}}{2h_x}, \delta_{\tilde{y}} v_{i,j} = \frac{v_{i,j+1} - v_{i,j-1}}{2h_y},\\
&\delta_x^2 v_{i,j} = \frac{v_{i+1,j} - 2v_{i,j} + v_{i-1,j}}{h_x^2}, \delta_y^2 v_{i,j} = \frac{v_{i,j+1} - 2v_{i,j} + v_{i,j-1}}{h_y^2},\\
&\mathcal{L}_x v_{i,j} = \left(1 + \frac{h_x^2}{12}\delta_x^2\right) v_{i,j} = \frac{v_{i+1,j} + 10v_{i,j} + v_{i-1,j}}{12},\\
&\mathcal{L}_y v_{i,j} = \left(1 + \frac{h_y^2}{12}\delta_y^2\right) v_{i,j} = \frac{v_{i,j+1} + 10v_{i,j} + v_{i,j-1}}{12}.
\end{aligned}$$

Let

$$\Delta_h = \mathcal{L}_x^{-1}\delta_x^2 + \mathcal{L}_y^{-1}\delta_y^2$$

be an approximation of the Laplacian operator Δ and it is easy to verify that the truncation error is $\mathcal{O}(h_x^4 + h_y^4)$. Define the mesh function

$$u = \{u_{ij}, i = 0, 1, \cdots, N_x - 1, j = 0, 1, \cdots, N_y - 1\}$$

and U is the finite difference approximation of u. (21) can be approximated by the following algebraic system

$$(I - \frac{2}{3}\Delta t\Delta_h)U = G.$$

Or equivalently,

$$\left(\mathcal{L}_x\mathcal{L}_y - \frac{2}{3}\Delta t(\mathcal{L}_y\delta_x^2 + \mathcal{L}_x\delta_y^2)\right) U = \mathcal{L}_x\mathcal{L}_y G. \tag{22}$$

The system can be written in the following operator splitting form

$$\left(\mathcal{L}_x - \frac{2}{3}\Delta t\delta_x^2\right)\left(\mathcal{L}_y - \frac{2}{3}\Delta t\delta_y^2\right) U = \mathcal{L}_x\mathcal{L}_y G + \mathcal{O}(\Delta t^2).$$

Instead of solving (22), we will compute the following approximate system

$$\mathcal{A}_h U = \left(\mathcal{L}_x - \frac{2}{3}\Delta t\delta_x^2\right)\left(\mathcal{L}_y - \frac{2}{3}\Delta t\delta_y^2\right) U = \mathcal{L}_x\mathcal{L}_y G,$$

which will be calculated through the two-step procedure

$$\begin{aligned}
&\left(\mathcal{L}_x - \frac{2}{3}\Delta t\delta_x^2\right) U^* = \mathcal{L}_x\mathcal{L}_y G,\\
&\left(\mathcal{L}_y - \frac{2}{3}\Delta t\delta_y^2\right) U = U^*.
\end{aligned} \tag{23}$$

This procedure requires solving a series of one-dimensional, tridiagonal systems. Define the discrete inner product

$$(U,V)_h = \sum_{i=0}^{N_x-1}\sum_{j=0}^{N_y-1} U_{i,j}V_{i,j}h_xh_y,$$

and the fourth-order approximation of the gradient operator

$$\nabla_h = \left(\delta_{\hat{x}}(I-\frac{h_x^2}{6}\delta_x^2),\ \delta_{\hat{y}}(I-\frac{h_y^2}{6}\delta_y^2)\right).$$

The spatially discretized system of (5) can be solved through the following steps:

(i) Compute γ_h^n with

$$\gamma_h^n = \frac{1}{3}\Delta t(b_{\phi,h}^n, V_1^n)_h + \frac{1}{3}\Delta t(b_{\psi,h}^n, V_2^n)_h + \frac{\alpha}{3\lambda}\Delta t(D_h^{n+1/2}\nabla_h b_{c,h}^n, \nabla_h b_{c,h}^n)_h, \tag{24}$$

where $D_h^{n+1/2} = D(\phi_h^{n+1/2})$. This requires solving the decoupled algebraic systems $\mathcal{A}_hV_1^n = b_{\phi,h}^n$ and $\mathcal{A}_hV_2^n = b_{\psi,h}^n$.

(ii) Compute θ_h^n with

$$\theta_h^n(1+\gamma_h^n) = (b_{\phi,h}^n, W_1^n)_h + (b_{\psi,h}^n, W_2^n)_h + (b_{c,h}^n, g_{c,h}^n)_h, \tag{25}$$

which requires to solve the decoupled algebraic systems $\mathcal{A}_hW_1^n = g_{\phi,h}^n$ and $\mathcal{A}_hW_2^n = g_{\psi,h}^n$.

(iii) Use $\theta_h^n, V_1^n, V_2^n, W_1^n$ and W_2^n found in (i) and (ii) to compute the solution $\phi_h^{n+1}, \psi_h^{n+1}, c_h^{n+1}$ by

$$\phi_h^{n+1} + \frac{1}{3}\Delta t V_1^n\theta_h^n = W_1^n, \tag{26}$$

$$\psi_h^{n+1} + \frac{1}{3}\Delta t\theta_h^n V_2^n = W_2^n, \tag{27}$$

and

$$\begin{aligned} c_h^{n+1} =& \frac{\alpha\theta_h^n}{3\lambda}\Delta t\nabla_h\cdot(D_h^{n+1/2}\nabla_h b_{c,h}^n) \\ &+ \frac{2\alpha}{3\lambda}\Delta t\nabla_h\cdot(D_h^{n+1/2}\nabla_h b_{c,h}^n)p_h^n + \frac{4}{3}c_h^n - \frac{1}{3}c_h^{n-1}. \end{aligned} \tag{28}$$

All the linear algebraic systems in steps (i) and (ii) can be solved by (23).

The fully discretized system of (6) can be obtained and solved in the same way as above.

Remark 1. *As SAV method guarantees unconditional energy stability, it is expected to derive the convergence of the numerical solution following the ideas introduced in* [6, 25, 22, 28]. *The theoretical analysis of convergence and error estimates will be included in the future work.*

4. Numerical tests

In this section, we test our scheme developed in previous sections with various numerical experiments on a two-dimensional rectangular domain $\Omega = [-l_x, l_x] \times [-l_y, l_y]$. The time and space step sizes of discretization are denoted by Δt and h, respectively. The ratio of steps is defined by $\mu = \Delta t/h^2$ that will be fixed during the tests.

4.1. Accuracy test. Firstly, we test the order of accuracy of our numerical method. The boundary condition is periodic and the initial condition is given by

$$\begin{cases} \phi_0(x,y) = \sin\left(\frac{\pi}{l_x}x\right)\sin\left(\frac{\pi}{l_y}y\right), \quad (x,y)\in\Omega, \\ \psi_0(x,y) = 0, \quad (x,y)\in\Omega, \\ c_0(x,y) = -0.25, \end{cases} \tag{29}$$

where $l_x = l_y = 0.5$ and the temperature is $T = -0.25$. The initial composition is negative since $C_0 < C_{p\beta}$. (See (2) for the definition of the scaled composition.) The spatial step is denoted by $h = h_x = h_y$ and we set the ratio of steps to be $\mu = 4.2 \times 10^{-3}$. Since the exact solution is unknown, we compute the order of convergence in space by $p = \log_2 \frac{\|u_{2h}-u_h\|_h}{\|u_h - u_{\frac{h}{2}}\|_h}$, where $\|\cdot\|_h^2 = (\cdot,\cdot)_h$ is the discrete L^2 norm on Ω, and the order of accuracy in time is then equal to $p/2$. The parameters of the model are listed in Table 1.

TABLE 1. Parameters of the phase field model.

λ	2.5	C_p	38.2 wt%	A_1	3.30745×10^{-1}
C_0	0	$C_{p\alpha}$	22.1 wt%	A_2	3.38509×10^{-1}
T_0	-0.2	$C_{p\beta}$	33.0 wt%	B_{11}	-2.56790×10^{-3}
α	1			B_{12}	-0.5
				B_{21}	-2.62818×10^{-3}
				B_{22}	0.0

It can be seen from Table 2 that as h decreases, the numerical solution converges at a order close to 4, which means the convergent order in time is close to 2. This result matches the accuracy order predicted in previous sections.

TABLE 2. Order of convergence.

$2h$	h	$\frac{h}{2}$	$\|u_{2h} - u_h\|$	$\|u_h - u_{\frac{h}{2}}\|$	Order
1/10	1/20	1/40	1.773647×10^{-2}	1.259232×10^{-3}	3.816104
1/20	1/40	1/80	9.265527×10^{-3}	6.194922×10^{-4}	3.902715
1/40	1/80	1/160	4.626094×10^{-3}	3.083850×10^{-4}	3.906990
1/80	1/160	1/320	2.312237×10^{-3}	1.540177×10^{-4}	3.908121
1/160	1/320	1/640	1.156018×10^{-3}	7.698638×10^{-5}	3.908417

4.2. Peritectic crystallization and energy stability. In this test, we simulate the peritectic crystallization on the domain $\Omega = [-20, 20] \times [-20, 20]$, where the initial state contains a piece of α-solid at the center that is surrounded by liquid of the alloy solution. Specifically, the initial values of the phase field model are given by

$$\phi_0(x,y) = \begin{cases} 1, & (x,y)\in[-2,2]\times[-2,2], \\ -1, & \text{otherwise}, \end{cases} \tag{30}$$

$$\psi_0(x,y) = \begin{cases} 1, & (x,y)\in[-2,2]\times[-2,2], \\ 0, & \text{otherwise}. \end{cases} \tag{31}$$

and

$$c_0 = -0.25.$$

The phase variable $\phi = 1$ is related to solid phase, and $\phi = -1$ is liquid. $\psi = 1$

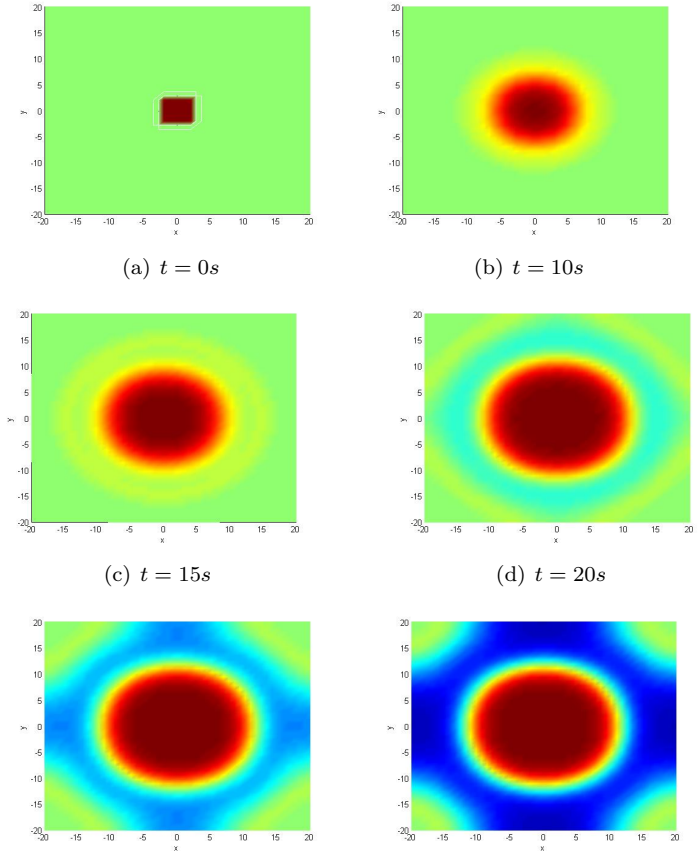

(a) $t = 0s$ (b) $t = 10s$

(c) $t = 15s$ (d) $t = 20s$

(e) $t = 22s$ (f) $t = 24s$

FIGURE 1. Peritectic crystallization. The initial liquid alloy solution (*green*) contains a piece of α-solid (*red*) in the center. The α-phase grows up and, after 20 seconds, β-phase (*blue*) starts to precipitate on the surface of α-phase to form peritectic crystal.

is related to α-solid and $\psi = -1$ is β-solid. The temperature is $T = -0.25$. As time goes on, the α-solid grows up and then a new phase, the β-solid, starts to precipitate on the surface of α-phase to form peritectic crystals (Fig. 1).

In the proof of stability, we calculate the discretized SAV free energy functional (18) as follows

$$E_h^{n+1} = \frac{1}{2}\left(|r^{n+1}|^2 + |2r^{n+1} - r^n|^2\right) + \frac{1}{4}\left(\|\nabla_h\phi^{n+1}\|_h^2 + \|2\nabla_h\phi^{n+1} - \nabla_h\phi^n\|_h^2\right) + \frac{1}{4}\left(\|\nabla_h\psi^{n+1}\|_h^2 + \|2\nabla_h\psi^{n+1} - \nabla_h\psi^n\|_h^2\right).$$

The change trend of free energy with time is shown in Fig. 2. With the increase of time, the free energy decreases gradually and tends to be stable.

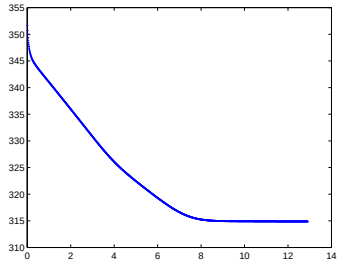

FIGURE 2. The change trend of discrete SAV free energy E_h^{n+1} with time.

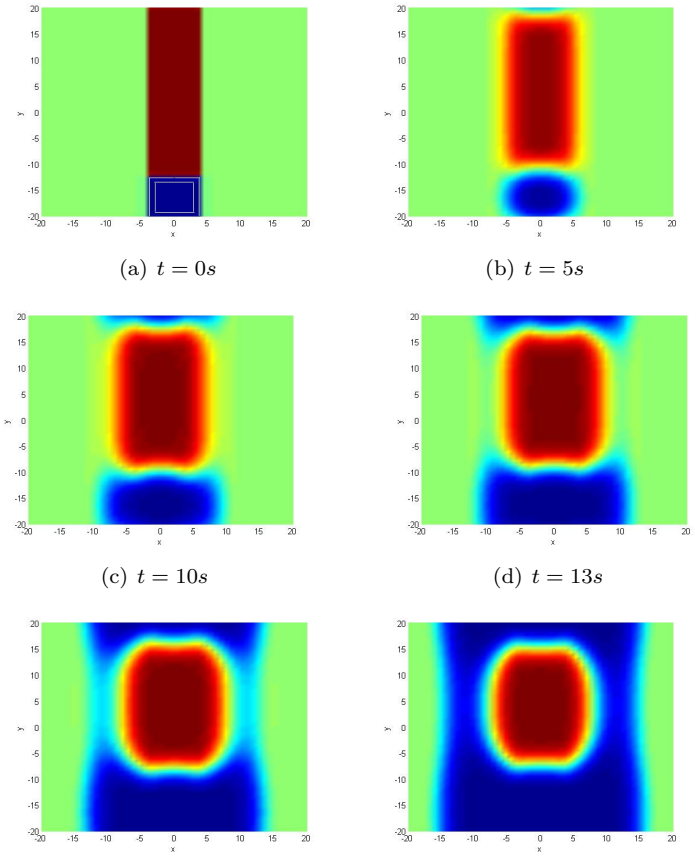

(a) $t = 0s$ (b) $t = 5s$

(c) $t = 10s$ (d) $t = 13s$

(e) $t = 16s$ (f) $t = 19s$

FIGURE 3. Development of a small β nucleus to bands. The triple-junction points keep moving upward until the β solids merge to form connected bands.

4.3. Simulations of morphological evolution. In this test, we simulate the peritectic solidification whose initial state contains a long strip of α-solid in middle of the alloy solution with a nucleus of β-solid at one end. When the reference temperature is held constant $T = -0.2$ and the initial composition is $c_0 = -0.21$, both α-phase and β-phase crystallize simultaneously. As β-solid grows faster than α-solid, the β nucleus eventually spreads around α solid to form band structures (Fig. 3).

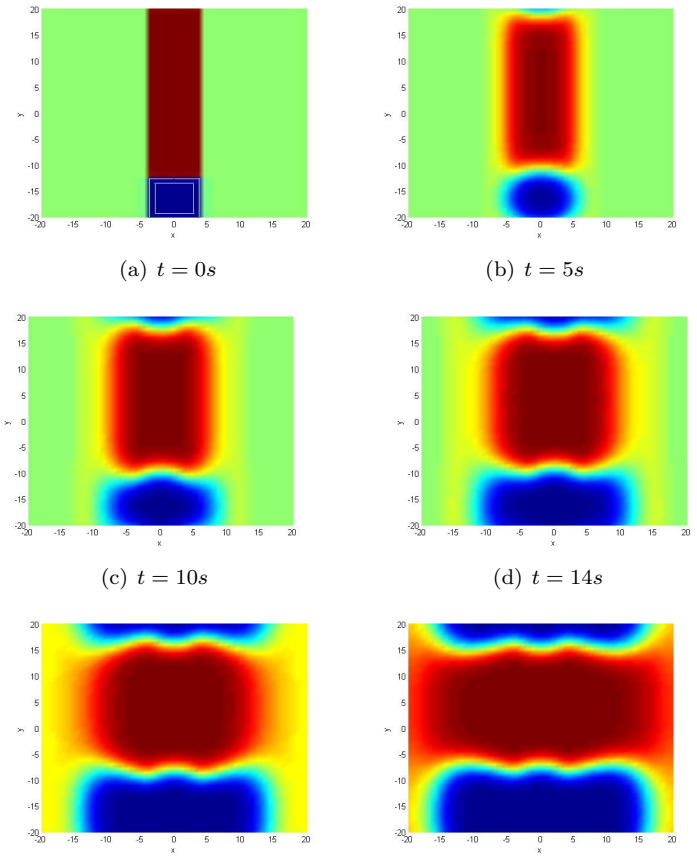

(a) $t = 0s$ (b) $t = 5s$

(c) $t = 10s$ (d) $t = 14s$

(e) $t = 18s$ (f) $t = 22s$

FIGURE 4. Development of a small β nucleus to islands. The trijunction points move up for a period of time and then turn down to form isolated islands when the initial composition has a gradient $c = c_0 - k|x|$.

Another structure, island, can also be observed when the initial composition, instead of being constant, has a gradient

$$c = c_0 - k|x|,$$

with $c_0 = -0.2, k = 0.0075$. As the β-phase grows up, the trijunction points move up to the left and right. However, after a period of time, the trijunction points turn around and isolated islands or partial bands are formed (Fig. 4).

5. Summary

We approximate a phase field model for peritectic crystallization with the scalar auxiliary variable (SAV) method in time. This method is linear, non-iterative and unconditionally energy-stable. The space variable is discretized by an operator splitting approach equipped with a high-order compact finite difference method which only requires solving a series of one-dimensional systems at each time step. Numerical experiments show accuracy, effectiveness and energy stability of our schemes. Other numerical methods, such as maximum bound principles preserving schemes [8, 9], for peritectic phase field models will be considered in the future.

Acknowledgments

The authors thank the anonymous referees for their valuable comments. S. Xie's work was partially supported by National Natural Science Foundation of China with grant number 11871443.

References

[1] G. Akrivis, B. Li, D. Li, Energy-decaying extrapolated RK-SAV methods for the Allen-Cahn and Cahn-Hilliard equations, SIAM J. Sci. Comput. 41 (2019) A3703-A3727.
[2] S. Badia, F. Guilln-Gonzlez, J.V. Gutirrez-Santacreu, Finite element approximation of nematic liquid crystal flows using a saddle-point structure, J. Comput. Phys. 230 (2011) 1686-1706.
[3] W. Chen, X. Wang, Y. Yan, Z. Zhang, A second order BDF numerical scheme with variable steps for the Cahn–Hilliard equation, SIAM J. Numer. Anal. 57.1 (2019) 495–525.
[4] K. Cheng, W. Feng, C. Wang, S. M. Wise, An energy stable fourth order finite difference scheme for the Cahn-Hilliard equation, J. Comput. Appl. Math. 362 (2019) 574-595.
[5] K. Cheng, C. Wang, S. M. Wise, A weakly nonlinear, energy stable scheme for the strongly anisotropic Cahn-Hilliard equation and its convergence analysis, J. Comput. Phys. 405 (2020) 109109.
[6] Q. Cheng, C. Wang, Error estimate of a second order accurate scalar auxiliary variable (SAV) numerical method for the epitaxial thin film equation, Adv. Appl. Math. Mech. 13 (2021) 1318-1354.
[7] Y. Cheng, A. Kurganov, Z. Qu, T. Tang, Fast and stable explicit operator splitting methods for phase-field models, J. Comput. Phys. 303 (2015) 45-65.
[8] Q. Du, L. Ju, X. Li, Z. Qiao, Maximum principle preserving exponential time differencing schemes for the nonlocal Allen-Cahn equation, SIAM J. Numer. Anal. 57 (2019) 875-898.
[9] Q. Du, L. Ju, X. Li, Z. Qiao, Maximum bound principles for a class of semilinear parabolic equations and exponential time differencing schemes, SIAM Rev. 63 (2021) 317-359.
[10] W. E, J. Liu, Essentially compact schemes for unsteady viscous incompressible flows, J. Comput. Phys. 126 (1996) 122-138.
[11] C. Elliott, A. Stuart, The global dynamics of discrete semilinear parabolic equations, SIAM J. Numer. Anal. 30 (1993) 1622-1663.
[12] D. Eyre, Unconditionally gradient stable time marching the Cahn-Hilliard equation, MRS. Proc. 529 (1998) 39-46.
[13] X. Feng, B. Li, S. Ma, High-order mass- and energy-conserving SAV-Gauss collocation finite element methods for the nonlinear Schrödinger equation, Preprint, (2020) arXiv: 2006.05073.
[14] Z. Gao, S. Xie, Fourth-order alternating direction implicit compact finite difference schemes for two-dimensional Schrödinger equations, App. Numer. Math. 61 (2011) 593-614.
[15] F. Guilln-Gonzlez, G. Tierra, On linear schemes for a Cahn-Hilliard diffuse interface model, J. Comput. Phys. 234 (2013) 140-171.
[16] X. Li, Z. Qiao, H. Zhang, Convergence of a fast explicit operator splitting method for the epitaxial growth model with slope selection, SIAM J. Numer. Anal. 55 (2017) 265-285.
[17] C. Liu, C. Wang, Y. Wang, A structure-preserving, operator splitting scheme for reaction-diffusion equations with detailed balance, J. Comput. Phys. 436 (2021) 110253.
[18] J. Liu, C. Wang, H. Johnston, A fourth order scheme for incompressible boussinesq equations, J. Sci. Comput. 18 (2003) 253-285.
[19] T. S. Lo, A. Karma, M. Plapp, Phase-field modeling of microstructural pattern formation during directional solidification of peritectic alloys without morphological instability, Phys. Rev. E 63 (2001) 031504.

[20] P. Mazumder, R. Trivedi, A. Karma, Phase transformations and systems driven far from equilibrium, MRS. SYM. Proc. 481 (1998) 39-44.
[21] B. Nestler, A. Wheeler, A multi-phase-field model of eutectic and peritectic alloys: numerical simulation of growth structures, Phys. D 138 (2000) 114-133.
[22] J. Shen, J. Xu, Convergence and error analysis for the scalar auxiliary variable(SAV) schemes to gradient flows, SIAM J. Numer. Anal. 56 (2018) 2895-2912.
[23] J. Shen, J. Xu, J. Yang, The scalar auxiliary variable (SAV) approach for gradient flows, J. Comput. Phys. 353 (2018) 407-416.
[24] J. Shen, J. Xu, J. Yang, A new class of efficient and robust energy stable schemes for gradient flows, SIAM. Rev. 61 (2019) 474-506.
[25] S. Sun, X. Jing, Q. Wang, Error estimates of energy stable numercial schemes for Allen-Cahn equations with nonlocal constraints, J. Sci. Comput. 79 (2019) 593-623.
[26] R. Trivedi, Theory of layered-structure formation in peritectic systems, Metall. Mater. Trans. A 26 (1995) 1583-1590.
[27] C. Wang, J. Liu, H. Johnston, Analysis of a fourth order finite difference method for the incompressible Boussinesq equations, Numer. Math. 97 (2004) 555-594.
[28] L. Wang, Y. Huang, K. Jiang, Error analysis of SAV finite element method to phase field crystal model, Numer. Math. Theor. Meth. Appl. 13 (2020) 372-399.
[29] A. A. Wheeler , G. B. McFadden, W. J. Boettinger, Phase-field model for solidification of a eutectic alloy, Proc. R. Soc. London. A (1996) 452-495.
[30] S. Xie, S. Yi, T. Kwon, Fourth-order compact difference and alternating direction implicit schemes for telegraph equations, Comput. Phys. Comm. 183 (2012) 552-569.
[31] X. Yang, Linear, first and second-order, unconditionally energy stable numerical schemes for the phase field model of homopolymer blends, J. Comput. Phys. 327 (2016) 294-316.
[32] X. Yang, D. Han, Linearly first- and second-order, unconditionally energy stable schemes for the phase field crystal model, J. Comput. Phys. 330 (2017) 1116-1134.
[33] C. Zhang, H. Wang, J. Huang, C. Wang, X. Yue, A second order operator splitting numerical scheme for the "good" Boussinesq equation, Appl. Numer. Math. 119 (2017) 179-193.
[34] J. Zhang, X. Yang, Decoupled, non-iterative, and unconditionally energy stable large time stepping method for the three-phase Cahn-Hilliard phase-field model, J. Comput. Phys. 404 (2020) 109115.
[35] J. Zhang, X. Yang, Unconditionally energy stable large time stepping method for the L^2-gradient flow based ternary phase-field model with precise nonlocal volume conservation, Comput. Methods Appl. Mech. Engrg. 361 (2020) 112743.
[36] G. Zhu, J. Kou, S. Sun, J. Yao, A. Li, Decoupled, energy stable schemes for a phase-field surfactant model, Comp. Phys. Commu. 233 (2018) 67-77.
[37] J. Zhu, L. Chen, J. Shen, V. Tikare, Coarsening kinetics from a variable mobility Cahn-Hilliard equation: application of semi-implicit Fourier spectral method, Phys. Rev. E 60 (1999) 3564-3572.

School of Mathematical Sciences, Ocean University of China, Qingdao, Shandong 266100, China
E-mail: 2543994245@qq.com

School of Mathematical Sciences, Ocean University of China, Qingdao, Shandong 266100, China
E-mail: shusenxie@ouc.edu.cn

School of Mathematical Sciences, Ocean University of China, Qingdao, Shandong 266100, China
E-mail: cgchen@ouc.edu.cn